BMC Medical Imaging

RESEARCH Open Access

Exploration of CT-based discrimination and diagnosis of various pathological types of ground glass nodules in the lungs

Haihui Wu[1*], Xiong Zhang[1] and Zheng Zhong[1]

Abstract

Purpose This study aims to examine the diagnostic usefulness of CT imaging in distinguishing between various pathological forms of lung ground-glass nodules (GGNs).

Methods We conducted a retrospective analysis on 210 patients with lung ground-glass nodules (GGNs) who received diagnosis and treatment at our hospital between January 2021 and May 2024. Every patient had comprehensive imaging and pathology investigations. Lesion size, three-dimensional ratio, two-dimensional ratio, size of solid components, form, spiculation, lobulation, and cavitation were studied across several pathological kinds of pulmonary ground-glass nodules (GGNs).

Results Of the 210 patients, 51 were diagnosed with benign conditions, while 159 had malignant lesions distributed across AIS, MIA, and IAC. The imaging data revealed that pulmonary ground-glass nodules (GGNs) exhibiting spiculation, lobulation, cavitation, pleural indentation, irregular shape, and fuzzy borders were considerably more prevalent in the inflammatory group, atypical adenomatous hyperplasia (AAH) group, adenocarcinoma in situ (AIS) group, minimally invasive adenocarcinoma (MIA) group, and invasive adenocarcinoma (IAC) group. These differences were statistically significant ($P < 0.05$). Significant variations in lesion size and size of solid components were observed among the groups, with the inflammatory group having the smallest size, followed by the AAH group, AIS group, MIA group, and finally the IAC group ($P < 0.05$). Nevertheless, there were no statistically significant disparities in the three-dimensional ratio and two-dimensional ratio across the five groups ($P > 0.05$). The calculated areas under the curve for distinguishing pre-invasive lesions from MIA and MIA from IAC, depending on the size of solid components, were 0.705 and 0.814, respectively. These values indicate a high diagnostic accuracy.

Conclusion A thorough examination of the CT imaging characteristics of ground-glass nodules is crucial for accurately distinguishing between various pathological forms of pulmonary GGNs.

Keywords Pulmonary ground-glass nodules, High-resolution CT, Pre-invasive lesions, Minimally invasive adenocarcinoma, Invasive adenocarcinoma, Differential diagnosis value

*Correspondence:
Haihui Wu
lin74074sci@163.com
[1]Meizhou People's Hospital, No. 63 Huangtang Road, Meijiang District, Meizhou, Guangdong 514031, China

Introduction

Ground-glass nodules (GGNs), an imaging concept, is defined as hazy opacity that does not obscure underlying bronchial structures or pulmonary vessels at high-resolution computed tomography (HRCT) [1]. The term "ground-glass opacities" is used because they resemble to ground glass. GGNs can exhibit either localized or diffuse distribution [2]. In clinical practice, chest CT exams are the gold standard in the detection. Research has indicated that recurring ground-glass nodules (GGNs) are frequently indicative of early-stage lung adenocarcinomas or precancerous lesions [3].

Lung adenocarcinoma is a form of non-small cell lung cancer that primarily affects women who do not smoke [4]. The incidence and mortality rates of lung adenocarcinoma have been increasing in recent years [5]. The initial manifestations of lung cancer are vague and might be easily disregarded. As the disease advances, the patient may have symptoms like hoarseness, swelling of the face and neck, and difficulty breathing. These symptoms can be life-threatening [6]. Therefore, timely detection of lung cancer is imperative. Due to the ongoing economic growth, rising living standards, and many variables such as lifestyle choices and the environment, the prevalence of lung adenocarcinoma is increasing. Moreover, it is now affecting younger age groups more frequently. In 2011, the International Association for the Study of Lung Cancer, the American Thoracic Society, and the European Respiratory Society categorized adenocarcinoma in situ (AIS) and atypical adenomatous hyperplasia (AAH) as pre-invasive lesions, while minimally invasive adenocarcinoma (MIA) and invasive adenocarcinoma (IAC) were classified as invasive lesions [7]. Imaging can detect focal ground-glass nodules, which can indicate both pre-invasive and invasive lesions. Research findings indicate that individuals with pre-invasive lesions had a 5-year survival rate of 100%, but the survival rate for invasive lesions ranges from 77.5 to 90% [8].

Precise characterization and classification of GGNs plays a crucial role in enabling clinicians to make well—founded decisions about treatment options and predict disease prognosis. CT parameters, including nodule dimensions, morphology, attenuation, border properties, and growth behavior, in conjunction with clinical variables and patient medical background, are crucial for precise diagnosis and risk evaluation. This article aims to present a comprehensive overview of ground-glass nodules, including their different pathological forms, as well as the obstacles involved in their CT diagnosis. We will examine the present comprehension of imaging characteristics that aid in distinguishing various disease entities inside GGNs.

Materials and methods

General data

A retrospective analysis was conducted on 210 patients with lung ground-glass nodules (GGNs) who were diagnosed and treated at our hospital between January 2021 and May 2024. Chest CT scans are a fundamental and routine diagnostic tool at Meizhou People's Hospital for patients with suspected pulmonary diseases. This imaging method is crucial for patients with potential GGNs, as it can effectively detect the presence, location, and certain characteristics of these nodules, which are often asymptomatic and discovered incidentally during scans. In this study, we focused on patients with confirmed GGNs to investigate the correlations between CT imaging features and pathological types.

The criteria for inclusion were as follows: (1) The presence of lung disease was established with CT scans and pathological exams. (2) A CT examination was conducted one month before to the surgery. (3) Blood routine tests showed normal findings. (4) There was a single lesion with a diameter smaller than 3 cm. (5) The study had access to comprehensive clinical data. The exclusion criteria encompassed the following conditions: (1) significant impairment of heart, liver, kidney, or other organs; (2) abnormalities in blood clotting; (3) contraindications for CT scanning; (4) congestive heart failure accompanied by other pathological conditions; (5) simultaneous presence of malignancies; (6) women who were breastfeeding or pregnant.

The Meizhou People's Hospital Review Board granted approval for this study.

CT scans

Each patient underwent CT scanning using the same Lian Ying 160-slice CT (model uCT780). The patients were placed in supine position, and the scanner parameters were modified to a current range of 220–250 milliamperes, voltage of 120 kilovolts, scanning thickness of 3 mm, and a detector configuration of 64×0.625 with a pitch of 1.016. The scans were conducted to capture the pulmonary system and its adjacent regions. For image reconstruction, when observing the pulmonary system, the window width (WW) was set to approximately 1500–1600 HU, and the window level (WL) was set to around – 500 to – 600 HU.

The acquisition of all pictures was done using non-contrast-enhanced plain scans. Image reconstruction was performed using both standard and high-resolution algorithms, in addition to parallel multi-plane reformation approaches.

Pathological diagnosis

All specimens for lung adenocarcinoma classification were procured via thoracoscopy or open chest biopsy,

as per the updated standards. The specimens were preserved in a solution of neutral formaldehyde, and all identified abnormalities were collected for further analysis. The samples were subsequently embedded in paraffin and processed into slides. For lesions with a diameter of ≤ 1.5 cm, the full section was used, whereas lesions larger than 1.5 cm were separated into halves. Hematoxylin and eosin (HE) staining was carried out as part of the regular procedure, and immunohistochemistry staining was undertaken for patients that presented diagnostic challenges.

The pathological diagnosis was conducted by two pathologists holding prominent professional positions. The diagnostic criteria were as follows [9]: (1) Atypical Adenomatous Hyperplasia (AAH): Small focal areas (diameter ≤ 0.5 cm) where epithelial cells show mild to moderate abnormal growth along the walls of the air sacs or respiratory bronchial tree, without any inflammation or fibrosis in the surrounding tissue; (2) Adenocarcinoma In Situ (AIS): Focal areas (diameter ≤ 3.0 cm) where tumor cells grow along the walls of the air sacs, without invading the surrounding tissue, blood vessels, or pleura; (3) Minimally Invasive Adenocarcinoma (MIA): Focal areas (diameter ≤ 3.0 cm) primarily characterized by tumor cells growing along the walls of the air sacs, with small invasive areas measuring ≤ 0.5 cm; (4) Invasive Adenocarcinoma (IAC): Focal areas (diameter ≤ 3.0 cm) with an invasive extent larger than 0.5 cm.

CT image evaluation

The lung window, with a window width of 1450–1500 HU and a window level of – 500 to 450 HU, reveals localized areas of increased density that do not obscure the bronchovascular bundles passing through them. These findings are specifically referred to as focused ground-glass opacities or ground-glass nodules. The lesions are categorized as either pure ground-glass nodules or mixed GGNs, based on their uniform density and the presence of soft tissue components. The quantification of the proportion of ground—glass components in mixed GGNs is conducted based on the ratio of ground—glass opacities in these nodules, as suggested by Aoki et al. [10]. This is done using the formula [(maximum diameter of ground-glass opacity—maximum diameter of solid component)/maximum diameter of ground-glass opacity] × 100%. The measurements of the maximum diameters are taken while avoiding blood vessels. The lesion's position and size are determined by measuring the maximum diameter A on the axial plane, the perpendicular short diameter B, and the superior-inferior diameter C on the coronal reconstructed image. The mean of these three measurements is considered as the lesion size. The following parameters are documented: two-dimensional ratio (A/B), three-dimensional ratio (A/C), density, morphology, margin characteristics (spiculation, lobulation), border characteristics, presence of air cavities, pleural retraction, and solid component (long diameter on the axial plane). The diagnosis is determined by two highly experienced chest radiologists, each with more than a decade of expertise, utilizing a blind review approach. In the event of any discrepancies, they are resolved by conversation.

Definition of imaging features

In the study of pulmonary ground—glass nodules (GGNs), precise definitions and inclusion criteria for key imaging features are crucial for accurate interpretation of differences among pathological groups.

Spiculation

Spiculation denotes fine, spikelike projections emerging from the GGN's margin. These spicules result from tumor cell infiltration or reactive fibrosis. On CT, they appear as short, linear densities radiating from the nodule.A nodule is classified as having spiculation if at least three distinct spikelike projections, each ≥ 2 mm long, are visible in at least two different planes and are distinguishable from normal pulmonary structures.

Lobulation

Lobulation is characterized by a non—smooth, lobulated nodule contour, resulting from differential growth rates within the lesion. It appears as a nodule composed of multiple small lobes. Lobulation is present when there are at least two distinct convexities on the nodule margin, with a ≥ 2 mm—deep indentation between them, visible in both axial and coronal planes.

Air bronchogram sign

The air bronchogram sign refers to the visualization of air—filled bronchi within the GGN. It occurs when abnormal tissue surrounds normal bronchi. On CT, it appears as branching, tubular lucencies inside the nodule. A nodule is positive for the air bronchogram sign if at least two continuous bronchial segments, following a normal branching pattern, are visible within the nodule on CT.

Pleural indentation sign

The pleural indentation sign is a triangular or linear pleural indentation towards the GGN, caused by lesion—induced traction. On CT, it shows as a focal pleural surface distortion. Pleural indentation is considered present when there is a distinct pleural indentation towards the nodule with an angle < 90 degrees and a length ≥ 3 mm, visible in at least one plane.

Lesion irregularity

Lesion irregularity implies deviation from a regular, round or oval shape. An irregular lesion has an uneven contour with protrusions or indentations, often due to heterogeneous growth or infiltration. A lesion is classified as irregular if the difference between its maximum and minimum diameters, measured in any two perpendicular planes, exceeds 20% of the average diameter.

Clear boundary

A clear boundary indicates a well—defined nodule margin, with a distinct transition from the nodule to the surrounding lung tissue. A nodule has a clear boundary if its edge can be clearly traced on CT, with ≤ 2 mm of blurring between the nodule and the lung tissue. In case of uncertainty, the consensus of two experienced radiologists is used for determination.

Statistical methods

Data analysis was performed using SPSS 25.0. Independent sample t-tests were used to analyze continuous data, and receiver operating characteristic (ROC) curves were constructed for the solid component. The area under the curve (AUC) was calculated. AUC values from 0.50 to 0.70 suggest limited diagnostic value, while values from 0.71 to 0.90 indicate moderate diagnostic value. Pearson chi-square and Fisher's exact tests were used to analyze categorical data. A significance level of $\alpha < 0.05$ was used.

Result

Diagnosis results

Out of the 210 patients who received a pathological investigation, 51 findings were determined to be benign. This includes 21 cases of pulmonary inflammation and 30 cases of atypical adenomatous hyperplasia (AAH), as shown in Fig. 1. A total of 159 lesions were identified as malignant, comprising 50 cases of adenocarcinoma in situ (AIS, Fig. 2), 65 cases of minimally invasive adenocarcinoma (MIA, Fig. 3), and 40 cases of invasive adenocarcinoma (IAC, Fig. 4). The CT diagnostic results indicated a positive predictive value of 98.74% (157 out of 159 cases), a negative predictive value of 90.19% (46 out of 51 cases), a sensitivity of 97.48% (155 out of 159 cases), and a specificity of 94.12% (48 out of 51 cases).

CT findings and diagnostic value

Pre-invasive lesions appear as pure ground-glass opacities, mostly round or oval, with relatively clear boundaries (Fig. 5); MIA can present as pure ground-glass opacities or mixed ground-glass opacities, also mostly round or oval, with relatively clear boundaries (Fig. 6); IAC is mostly mixed-density ground-glass opacities, often irregular in shape (Fig. 7). Univariate analysis of variance showed no statistically significant differences in age and BMI among the groups ($P > 0.05$); categorical data showed that spiculation, lobulation, air bronchogram sign, pleural indentation sign, irregularity of the lesion, and clear boundary showed statistically significant differences among the groups, with the inflammation

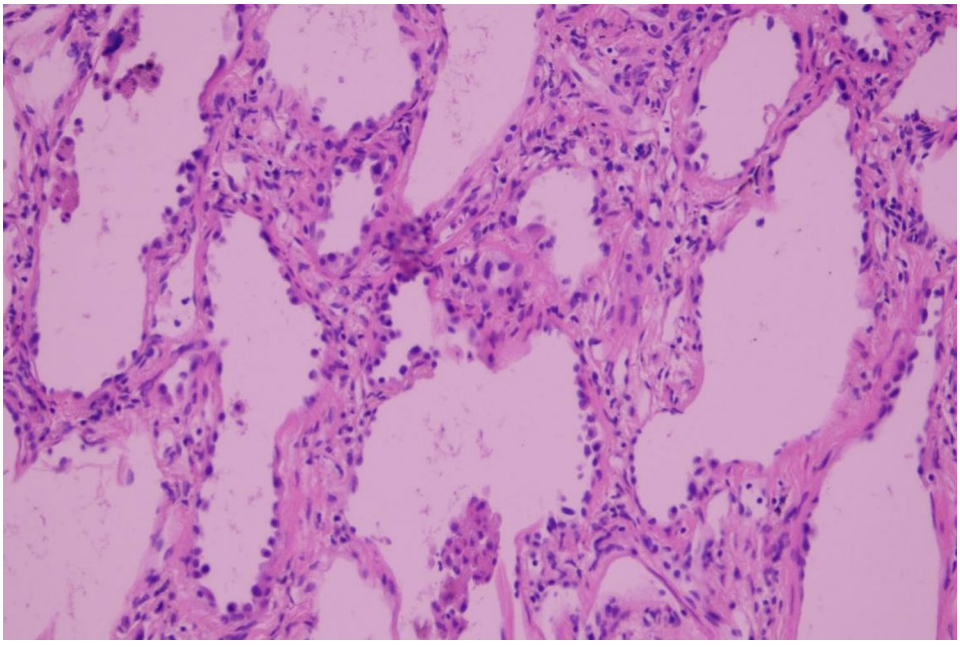

Fig. 1 Atypical adenomatous hyperplasia (AAH), Hematoxylin and Eosin staining

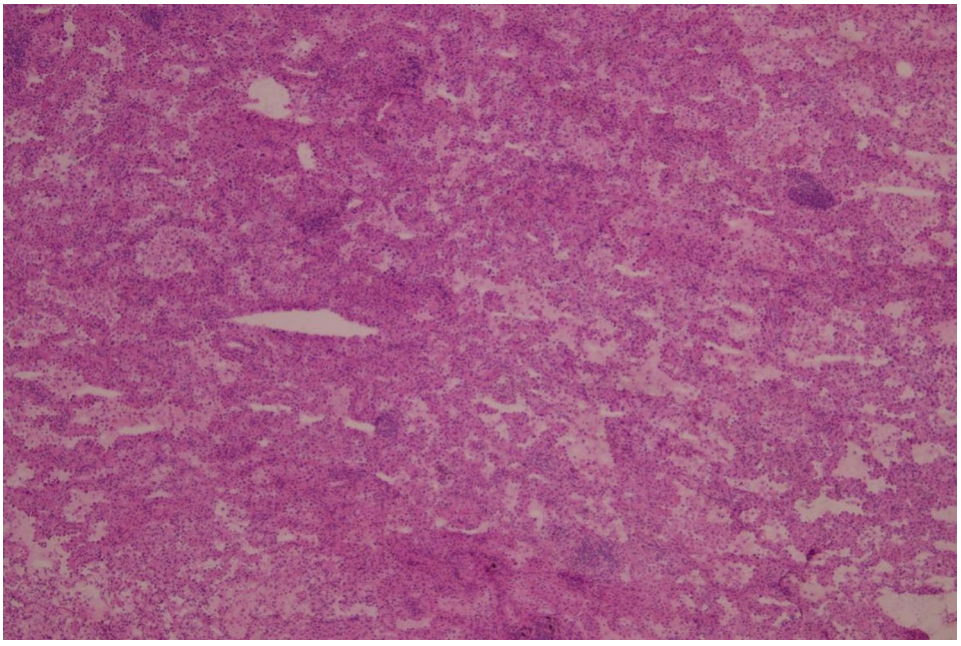

Fig. 2 Adenocarcinoma in situ (AIS), Hematoxylin and Eosin staining. Note: Non-mucinous type, tumor cells grow along the alveolar walls in a hugging pattern, without interstitial or vascular infiltration, and the alveolar cavities contain air

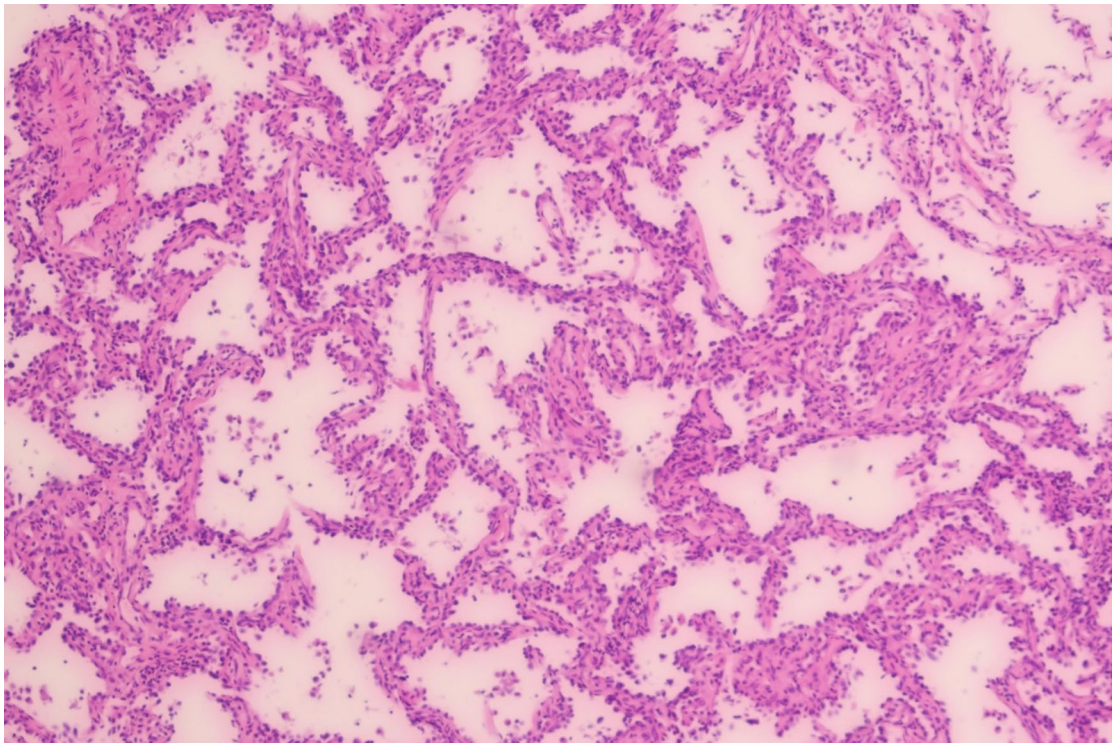

Fig. 3 Minimally invasive adenocarcinoma (MIA). Note: Non-mucinous type, tumor cells primarily grow along the alveolar walls in a hugging pattern, with infiltration foci ≤ 0.5 cm. Widened alveolar septa show fibrous components stimulated by tumor proliferation, and a small amount of tumor cells can be seen within the alveolar cavities

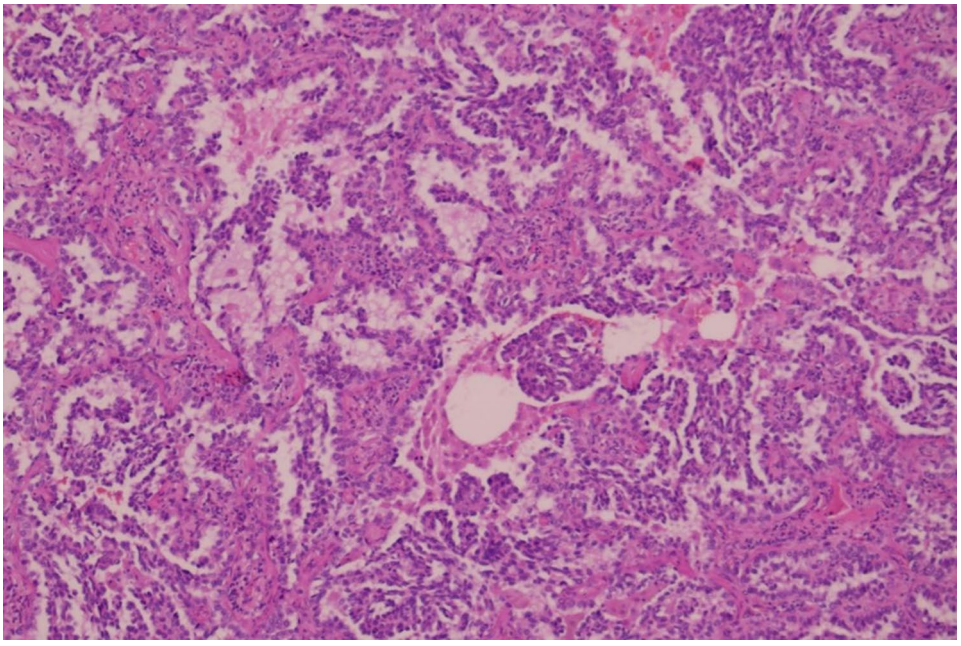

Fig. 4 Invasive adenocarcinoma (IAC). Note: The tumor cells exhibit multilayered growth and can be observed stimulating fibrous proliferation. The infiltration foci are larger than 0.5 cm, and there is a reduction in air content within the alveolar cavities

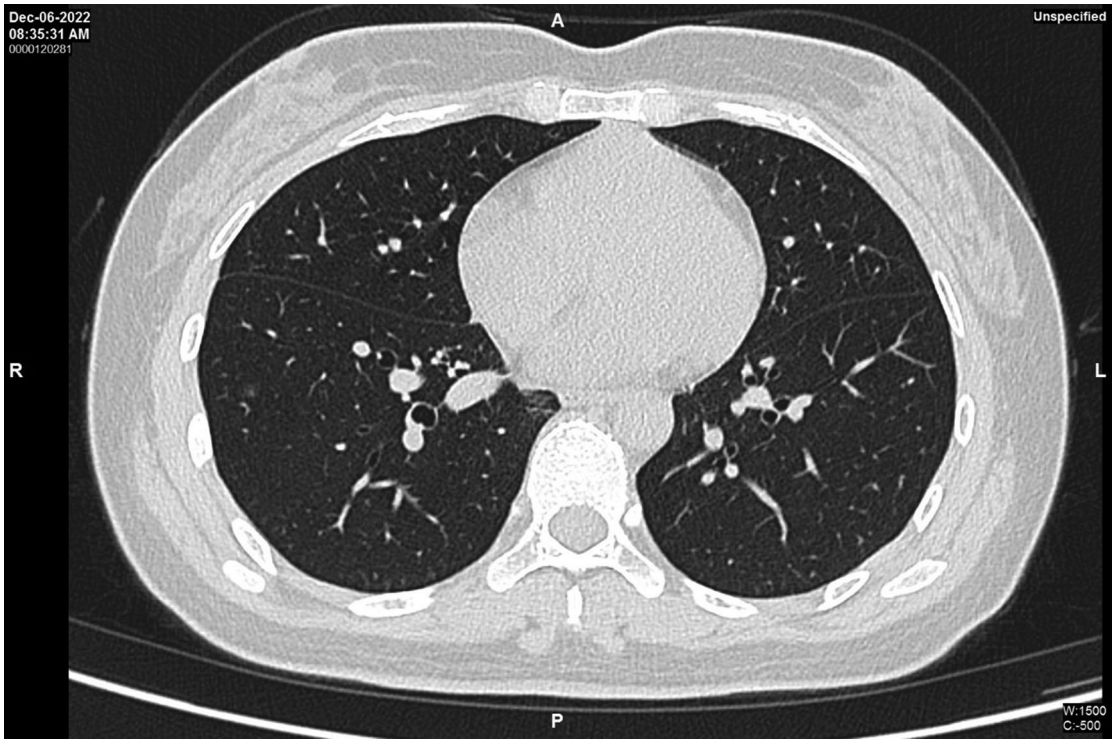

Fig. 5 CT image of adenocarcinoma in situ. This is a CT image of adenocarcinoma in situ, which appears as a round or oval pure ground glass nodule with clear boundaries and no obvious solid components, reflecting the pathological characteristics of the tumor growing along the alveolar wall without infiltration

group < AAH group < AIS group < MIA group < IAC group ($P < 0.05$). See Table 1 for details.

Comparison of size and solid component ratio of GGN lesions in different pathological types

The results showed that there were statistically significant differences in lesion size and solid component size

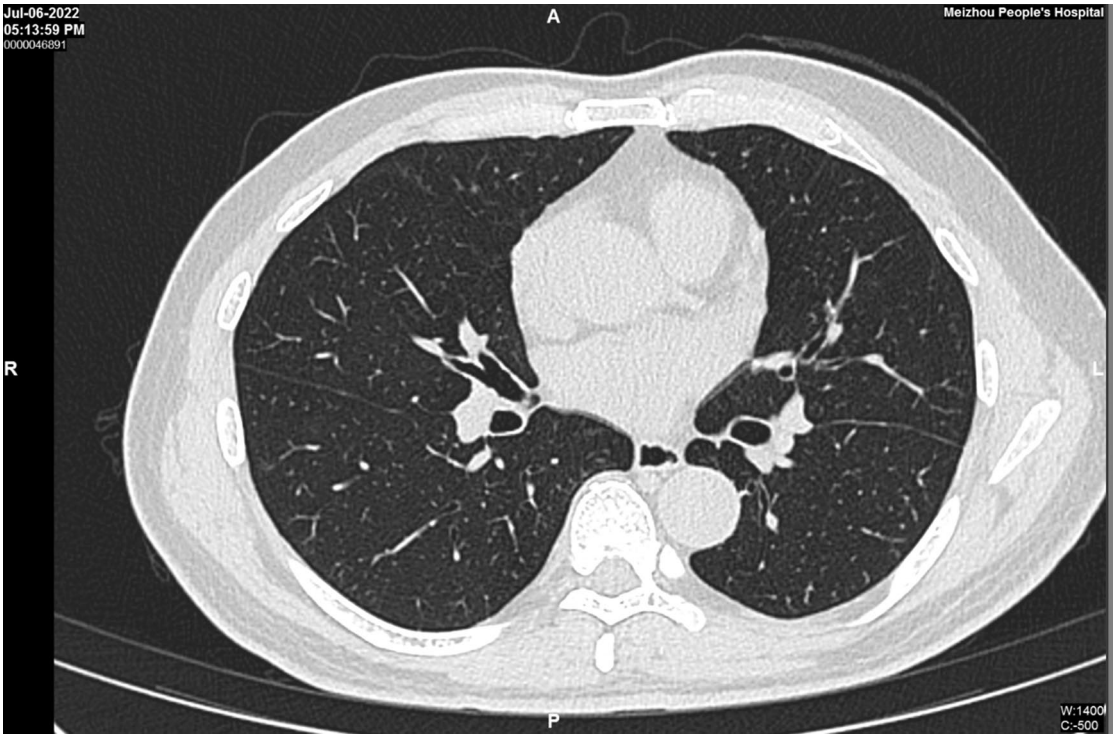

Fig. 6 CT image of minimally invasive adenocarcinoma. This figure shows the CT manifestations of minimally invasive adenocarcinoma, which may be pure ground glass nodules or mixed ground glass nodules, which are mostly round or oval with clear boundaries. If there are solid components, it indicates the presence of a small area of infiltration

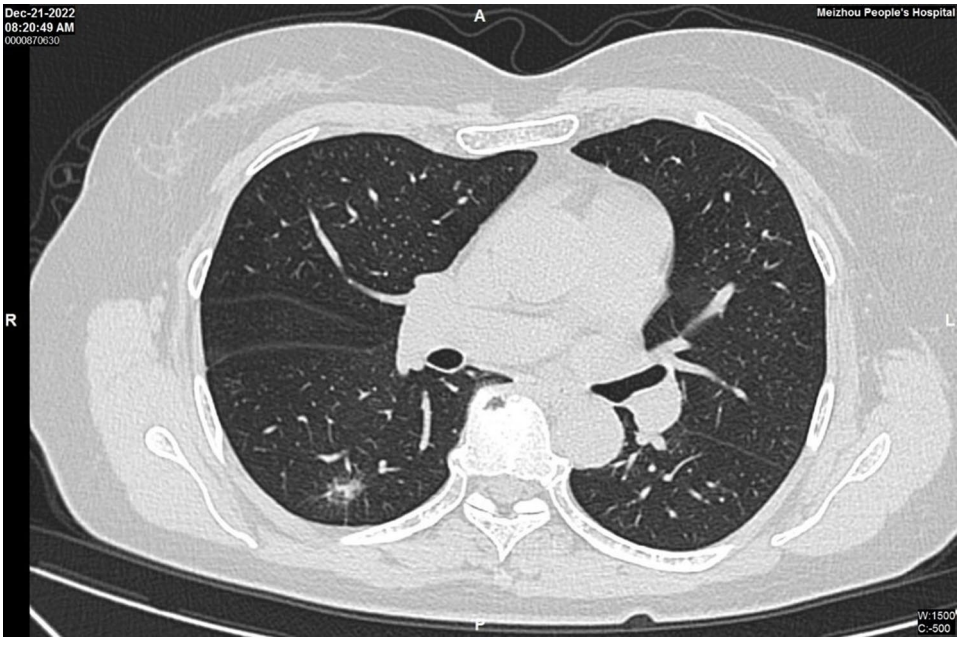

Fig. 7 CT image of invasive adenocarcinoma. This CT image shows invasive adenocarcinoma, which is mostly mixed-density ground-glass nodules with irregular morphology and obvious solid components, reflecting the characteristics of invasive tumor growth, and imaging features such as lobulation and spiculation can be seen

Table 1 Comparison of pathological data of different pathological types of pulmonary GGN [x ± s, n]

		Inflammation group (n = 21)	AAH group (n = 30)	AIS group (n = 50)	MIA group (n = 65)	IAC group (n = 44)	F/x^2	*P*
Gender (Male/Female)		9/12	7/23	16/34	34/31	14/30	0.060	0.806
Age		57.1 ± 5.9	52.6 ± 6.0	53.6 ± 6.2	55.4 ± 6.1	56.5 ± 6.3	0.047	0.996
BMI (kg/m^2)		23.2 ± 3.1	23.3 ± 3.0	23.4 ± 3.2	23.3 ± 3.2	23.5 ± 3.3	0.017	0.999
Peritumoral margin	Glitch	0	1	3	18	15	31.174	<0.001
	Leaf	0	0	12	32	24	45.142	<0.001
Symptoms around the lesion	Cavitation sign	1	2	7	12	23	33.462	<0.001
	Vascular bundle sign	0	0	1	11	7	19.426	<0.001
	Pleural indentation sign	0	2	5	17	15	11.871	0.001
Lesion shape	Circle, regular	18	20	22	28	12	24.797	<0.001
	Irregular	3	10	28	37	32	24.797	<0.001
Boundary	Clear	3	25	35	46	20	38.526	<0.001

Table 2 Comparison of the size and solid components of pulmonary GGN lesions in different pathological types

Category	Inflammation group	AAH group	AIS group	MIA group	IAC group	F	*P*
Lesion size (mm)	8.5 ± 1.5	9.0 ± 1.0	10.0 ± 1.5	12.0 ± 2.0	15.0 ± 2.5	116.54	<0.001
three-dimensional ratio	1.0 ± 0.1	1.1 ± 0.1	1.1 ± 0.2	1.2 ± 0.1	1.3 ± 0.2	6.98	0.001
two-dimensional ratio	1.4 ± 0.2	1.3 ± 0.3	1.5 ± 0.2	1.4 ± 0.3	1.6 ± 0.4	4.23	0.03
Solid composition (mm)	0.0 ± 0.0	0.5 ± 0.5	1.0 ± 0.5	3.5 ± 1.0	7.0 ± 1.5	354.57	<0.001

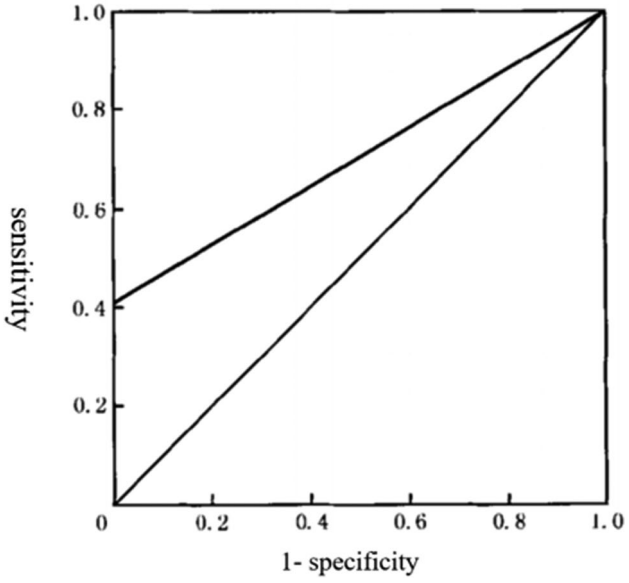

Fig. 8 Receiver operating characteristic (ROC) curve for the solid component of pre-invasive lesions and microinvasive cancer lesions

among the groups, with the inflammation group < AAH group < AIS group < MIA group < IAC group ($P < 0.05$). However, there were no statistically significant differences in the three-dimensional ratio and two-dimensional ratio among the five groups ($P > 0.05$). Please refer to Table 2 for details.

ROC curve analysis

We plotted receiver operating characteristic (ROC) curves based on the size of solid components in ground-glass nodules (GGNs). For distinguishing pre-invasive lesions from minimally invasive adenocarcinoma (MIA), the area under the curve (AUC) of the ROC curve was 0.705, indicating moderate diagnostic value. When classifying nodules with solid components 1 mm or larger as MIA, the sensitivity was 41.0% and the specificity was 100% (Fig. 8).

When differentiating between MIA and invasive adenocarcinoma (IAC), the AUC of the ROC curve was 0.814, also showing moderate diagnostic value. When categorizing nodules with solid components 3 mm or larger as IAC, the sensitivity was 67.7% and the specificity was 87.2%. When classifying nodules with solid components 6 mm or larger as IAC, the sensitivity was 64.7% and the specificity was 100% (Fig. 9).

Discussion

GGN is a radiographic feature of the lungs that is closely associated with early lung adenocarcinoma. Therefore, improving the examination of GGN is a key point in the screening and treatment of early lung adenocarcinoma. The correlation between the imaging features of ground-glass nodules (GGNs) and pathological diagnosis has become a hot topic in recent years. GGNs can represent benign lesions such as infection, inflammation, and focal fibrosis, as well as pre-cancerous lesions such as atypical adenomatous hyperplasia (AAH) and adenocarcinoma in situ (AIS), and even different grades of lung

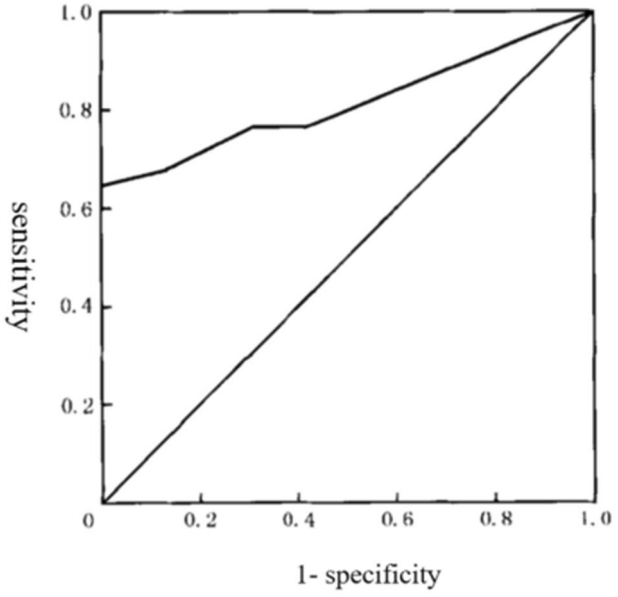

Fig. 9 Receiver Operating Characteristic (ROC) curve for the solid component of microinvasive cancer and invasive adenocarcinoma lesions

adenocarcinoma such as minimally invasive adenocarcinoma (MIA) and invasive adenocarcinoma (IAC) [11].

Under normal conditions, the alveolar cavities are filled with gas. In pathological conditions, when there is fluid retention, granulation tissue formation, or tumor infiltration in the alveolar cavities, the increased density of local lung tissue leads to a decrease in gas content within each pixel on the CT image, resulting in the appearance of ground-glass opacities. Histologically, AAH, AIS, and MIA all originate from type II pneumocytes or Clara cells and tend to grow along the alveolar walls and the inner surface of respiratory bronchioles [12]. When there is no peripheral infiltration or collapse of alveoli, or only thickening of the alveolar walls, a small amount of mucus, and desquamated tumor cells within the alveolar cavities, the CT image appears as pure ground-glass nodules. When tumor cells accumulate locally in multiple layers or are accompanied by infiltration, alveolar wall collapse, and reactive fibrous proliferation, the nodules appear as mixed ground-glass opacities. In our study, the pre-invasive lesions showed pure ground-glass nodules on CT images, while most IACs showed mixed ground-glass opacities. However, there were also some cases of MIA and IAC that appeared as pure ground-glass nodules. This may be due to the limited resolution of CT and differences in lung tissue inflation, resulting in discrepancies between the extent of lesion infiltration observed on CT images and under a microscope. Furthermore, if the tumor cells growing along the bronchiolar walls are multi-layered or show other histological subtypes such as acinar, papillary, micropapillary, and solid patterns, or if the tumor cells infiltrate the muscular fibrous stroma, even without alveolar distension, the infiltration can still be assessed. However, in these cases, there is still a relatively large amount of gas within the alveoli, and the density within each pixel does not reach a certain level, so the CT image still appears as pure ground-glass nodules.

In our study, both pre-invasive lesions and MIA predominantly showed a round or oval shape, while IACs showed an irregular shape. Pathologically, AIS and MIA tend to grow along the alveolar walls without significant infiltration, resulting in a round or oval shape. If tumor cell infiltration is evident and there are differences in cellular differentiation, growth rates, or contraction of fibrous tissue within different parts of the tumor, the shape tends to become irregular, which is frequently observed in IACs. Our results showed that the three-dimensional ratio of pre-invasive lesions, MIA, and IAC was close to 1, indicating that the lesions exhibited expansive growth in all directions, resulting in a predominantly spherical shape on three-dimensional imaging.

The boundaries of pre-invasive lesions and MIA were mostly well-defined, indicating the absence of a transitional zone or transition zone between the lesion and normal lung tissue. This is due to the weak invasiveness of the lesions or the strong defense mechanism of normal lung tissue. However, as tumor infiltrative growth increases, the boundaries tend to become more irregular.

The presence of spiculations, lobulations, air-filled spaces within the lesion, and pleural indentation signs are highly valuable for diagnosing solid malignant solitary pulmonary nodules. However, in our study, the rates of these features were not high for pre-invasive lesions and MIA, which may be due to the early stage and less invasive nature of these lesions, resulting in the absence of obvious malignant characteristics. Additionally, the contrast between ground-glass opacity and normal lung tissue on CT images is relatively weak, which inevitably affects the evaluation of some features. However, the rates of these features in IAC were higher than those in MIA and pre-invasive lesions, which is consistent with the gradual increase in tumor invasiveness from pre-invasive lesions to MIA and then to IAC. There are different views regarding the diagnostic value of lesion size for the pathological type of the lesion. In our study, IAC was significantly larger than MIA, but in clinical practice, some MIA lesions may be larger than IAC lesions. Therefore, relying solely on lesion size as a basis for differential diagnosis is unreliable.

AAH, MIA, and IAC are part of a dynamic process involving multiple genes. The amount of solid component within mixed ground-glass opacities can serve as an indicator of malignancy and invasiveness. The greater the proportion of solid component, the higher the likelihood of malignancy. If the lesion is malignant, a greater

proportion of solid component indicates greater invasiveness. These findings are consistent with previous reports, and there were statistically significant differences in the amount of solid component among the groups.

The lymph node metastasis rate is extremely low in patients with AIS and MIA, and they have a good prognosis if they undergo curative surgery. Although both MIA and IAC are invasive adenocarcinomas, they differ significantly in terms of lesion size, lymph node metastasis rate, surgical scope, and prognosis. Therefore, it is important to timely and accurately diagnose MIA and prevent progression to IAC. The results of this study indicate that there is not much morphological difference between pre-invasive lesions and MIA, while there are some similarities and differences in morphology between MIA and IAC. The size of solid components within the lesions is valuable for differential diagnosis. If a solid component ≥ 5 mm is used as the threshold for diagnosing IAC, the sensitivity is 67.7%, and the specificity is 87.2%. If I > 6 mm is used as the threshold, the sensitivity is 64.7%, and the specificity is 100%. This is very close to the definition of MIA and IAC in the 2011 lung adenocarcinoma classification, which uses 5 mm as the threshold for lesion infiltration. Therefore, the presence of solid components within the lesion can be used as one of the criteria for differentiating the degree of infiltration. Pure ground-glass nodules shown on CT are mostly AAH, AIS, or MIA. When there is an increase in solid components within the ground-glass nodule, it tends to lean towards a diagnosis of MIA or IAC. If the longest diameter of the solid component within the lesion is ≥ 5 mm, especially > 16 mm, it highly suggests IAC. For follow-up ground-glass nodules, if new solid components appear or existing solid components increase in size, caution should be exercised as it indicates disease progression. It is recommended that patients undergo puncture biopsy or surgical resection for pathological diagnosis in a timely manner [11].

Our study on using the size of solid components in ground-glass nodules (GGNs) is aligned with the broader evidences in medical image analysis research. In the context of multi-site medical image segmentation, the work of You et al. introduced the incremental-transfer learning (ITL) framework in their research. This framework, which learns from multi-site datasets in an end-to-end sequential fashion, could potentially be applied to our GGN analysis. By leveraging sequential learning and transfer of information, ITL might help in better generalizing the diagnosis of GGNs across different datasets and imaging sites [13]. In semi-supervised medical image segmentation, the SimCVD framework proposed by You et al. offers valuable insights. Our GGN study might benefit from its unsupervised training strategy and structural distillation approach. Given the often limited labeled data in medical imaging, the ability of SimCVD to achieve good performance with less labeled data could be applied to improve the accuracy of GGN diagnosis, especially in identifying the solid components and their associated pathological types [14]. For 2D medical image segmentation, the CASTformer presented by You et al. addresses several limitations of existing transformer-based models. Its use of a pyramid structure for multi-scale representations and a class-aware transformer module for learning discriminative regions could be adapted to our GGN analysis. By better capturing the features of GGNs at different scales and understanding the semantic contexts related to the solid components, we might enhance the accuracy of distinguishing between pre-invasive lesions, minimally invasive adenocarcinoma (MIA), and invasive adenocarcinoma (IAC), similar to how CASTformer outperformed previous approaches in its benchmarks [15].

This study has multiple limitations. It is retrospective, has a small sample size, is single—centered, and may have interobserver variability in radiological interpretation. There's a lack of long—term follow—up, full pathological confirmation for all cases, and potential confounding factors. Also, the exclusion of patients with multiple nodules should be noted. Future research should use larger cohorts, adopt prospective designs, standardize assessment methods, and ensure comprehensive pathological confirmation to validate and improve the findings.

To summarize, the radiographic features of ground-glass nodules, including size, shape, boundaries, presence of spiculations or lobulations and amount of solid component, can provide valuable information for the differential diagnosis of pre-invasive lesions, MIA, and IAC in lung adenocarcinoma. Early detection and accurate diagnosis of these lesions are crucial for implementing appropriate treatment strategies and improving patient outcomes.

Acknowledgments
Not applicable.

Author contributions
HW wrote the main manuscript. HW and XZ prepared the data collection. XZ and ZZ prepared figures and tables. HW and ZZ analyse and interpret of results. All authors reviewed the results and approved the final version of the manuscript. All authors would be informed each step of manuscript processing including submission, revision, revision reminder, etc.

Funding
The work was not funded by any funding.

Data availability
The datasets used and analysed during the current study available from the corresponding author on reasonable request.

Declarations

Ethics approval and consent for publication
This study was approved by the Ethics Committee of the Meizhou People's Hospital (Meizhou City Review 2023-C-136). Informed consent was obtained

from all the participants. All methods were carried out in accordance with Declaration of Helsinki.

Consent for publication
All the authors confirming that WRITTEN INFORMED consent was obtained from all subjects and/or their legal guardian(s).

Clinical trial number
Not applicable.

Competing interests
The authors declare no competing interests.

Received: 12 November 2024 / Accepted: 28 March 2025
Published online: 14 April 2025

References

1. Fu F, Zhang Y, Wang S, et al. Computed tomography density is not associated with pathological tumor invasion for pure ground-glass nodules. J Thoracic Cardiovasc Surg 2021;162:451–459.e453.
2. Jung J, Hong H, Goo JM. Ground-glass nodule segmentation in chest CT images using asymmetric multi-phase deformable model and pulmonary vessel removal. Comp Biol Med. 2018;92:128–38.
3. Fu G, Yu H, Liu J, et al. Arc concave sign on thin-section computed tomography: a novel predictor for invasive pulmonary adenocarcinoma in pure ground-glass nodules. Eur J Radiol. 2021;139:109683.
4. Saito S, Espinoza-Mercado F, Liu H, et al. Current status of research and treatment for non-small cell lung cancer in never-smoking females. Cancer Biol Therapy 2017;18:359–68.
5. Byers LA, Rudin CM. Small cell lung cancer: where do we go from here? Cancer. 2015;121(5):664–72.
6. Ahn S, Hwang SH, Han J, et al. Transformation to small cell lung cancer of pulmonary adenocarcinoma: clinicopathologic analysis of six cases. J Pathol Transl Med 2016;50:258–63.
7. Kitami A, Sano F, Hayashi S, et al. Correlation between histological invasiveness and the computed tomography value in pure ground-glass nodules. Surg Today. 2016;46:593–98.
8. Bongiolatti S, Corzani R, Borgianni S, et al. Long-term results after surgical treatment of the dominant lung adenocarcinoma associated with ground-glass opacities. J Thoracic Dis 2018;10:4838.
9. Lazarus DR, Strange CD, Ahuja J, et al. Non-small cell carcinoma. The thorax: medical, radiological, and pathological assessment. Berlin: Springer; 2023. p. 311–72.
10. Aoki T. Predicting factors of ground-glass lung nodule for growth. J Thoracic Dis 2018;10(Suppl 33):S3927.
11. Divisi D, Barone M, Zaccagna G, et al. Fluorine-18 fluorodeoxyglucose positron emission tomography in the management of solitary pulmonary nodule: a review. Ann Med 2017;49:626–35.
12. Shi Y-X, Shi X-D, Wang L-W, et al. Complications and image findings. In: Avian influenza human. Berlin: Springer. 2021. p. 71–83.
13. You C, Xiang J, Su K, et al. Distributed, collaborative, and federated learning, and affordable AI and healthcare for resource diverse global health. In: Lecture Notes in Computer Science. Cham: Springer. 2022. p. 3–16.
14. You C, Zhou Y, Zhao R, et al. SimCVD: simple contrastive voxel-wise representation distillation for semi-supervised medical image segmentation. Piscataway: IEEE; 2022.
15. You C, Zhao R, Liu F, et al. Class-aware adversarial transformers for medical image segmentation. Advances in neural information processing systems 35 (NeurIPS 2022) Main Conference Track, 2022.

Publisher's Note